Reconsidering tympanal-acoustic interactions leads to an improved model of auditory acuity in a parasitoid fly

Bioinspiration & Biomimetics

PAPER

Reconsidering tympanal-acoustic interactions leads to an improved model of auditory acuity in a parasitoid fly

Max R Mikel-Stites[1,2,3], Mary K Salcedo[1], John J Socha[1], Paul E Marek[4] and Anne E Staples[1,2,*]

[1] Department of Biomedical Engineering and Mechanics, Virginia Tech, Blacksburg, VA 24061, United States of America
[2] Engineering Mechanics program, Virginia Tech, Blacksburg, VA 24061, United States of America
[3] Department of Mathematics, Virginia Tech, Blacksburg, VA 24061, United States of America
[4] Department of Entomology, Virginia Tech, Blacksburg, VA 24061, United States of America
[*] Author to whom any correspondence should be addressed.

E-mail: staplesa@vt.edu

Keywords: acoustics, binaural hearing, biomechanics, mathematical modeling, sensory modeling, *Ormia ochracea*, bioinspiration

Supplementary material for this article is available online

OPEN ACCESS

RECEIVED
9 November 2022

REVISED
9 February 2023

ACCEPTED FOR PUBLICATION
28 February 2023

PUBLISHED
5 April 2023

Abstract

Although most binaural organisms locate sound sources using neurological structures to amplify the sounds they hear, some animals use mechanically coupled hearing organs instead. One of these animals, the parasitoid fly *Ormia ochracea* (*O. ochracea*), has astoundingly accurate sound localization abilities. It can locate objects in the azimuthal plane with a precision of 2°, equal to that of humans, despite an intertympanal distance of only 0.5 mm, which is less than 1/100th of the wavelength of the sound emitted by the crickets that it parasitizes. *O. ochracea* accomplishes this feat via mechanically coupled tympana that interact with incoming acoustic pressure waves to amplify differences in the signals received at the two ears. In 1995, Miles *et al* developed a model of hearing mechanics in *O. ochracea* that represents the tympana as flat, front-facing prosternal membranes, though they lie on a convex surface at an angle from the flies' frontal and transverse planes. The model works well for incoming sound angles less than ±30° but suffers from reduced accuracy (up to 60% error) at higher angles compared to response data acquired from *O. ochracea* specimens. Despite this limitation, it has been the basis for bio-inspired microphone designs for decades. Here, we present critical improvements to this classic hearing model based on information from three-dimensional reconstructions of *O. ochracea*'s tympanal organ. We identified the orientation of the tympana with respect to a frontal plane and the azimuthal angle segment between the tympana as morphological features essential to the flies' auditory acuity, and hypothesized a differentiated mechanical response to incoming sound on the ipsi- and contralateral sides that depend on these features. We incorporated spatially-varying model coefficients representing this asymmetric response, making a new quasi-two-dimensional (q2D) model. The q2D model has high accuracy (average errors of under 10%) for all incoming sound angles. This improved biomechanical model may inform the design of new microscale directional microphones and other small-scale acoustic sensor systems.

Abbreviations

The following abbreviations are used in this manuscript:

ITD	interaural time delay
IAD	interaural amplitude difference (sometimes called the interaural intensity difference (IID) or interaural level difference (ILD))
mITD	mechanical interaural time delay
mIAD	mechanical interaural amplitude difference

1. Introduction

The ability to localize sound allows animals to avoid predators and assists them in finding mates

and capturing prey. Binaural organisms locate sound-emitting objects by comparing the intensity and timing of incident sound waves arriving at their two hearing organs (figure 1(A)). Sound localization in binaural organisms is commonly described using two metrics: the ITD, the difference in the time it takes sound to reach the two hearing organs, and the IAD, the difference in sound amplitude between the two organs figure 1(A) [1]. Once a sound wave has reached an organism, IAD and ITD typically depend primarily on the animal's size. Larger-headed animals generally have larger ITD values due to the greater distance between their hearing organs.

Larger animals also have larger IAD values due to acoustic shading by their heads when the sound wavelength is comparable to or smaller than their head size, and to the lower amplitude of the acoustic signal at the ear farther from the sound source, since sound decays as $1/r^2$. When the animal is located at a great enough distance from the sound source, acoustic decay can reduce the amplitude of incoming sound below the threshold for acoustic sensing on one side or both.

The particulars of sound localization are complex and vary widely among animals, as the ITD and IAD ranges experienced by binaural animals demonstrate (figure 1(B)). In vertebrates, ITD is calculated in the brain stem's superior olivary nucleus, and IAD is calculated in the inferior colliculus in the midbrain nucleus [2]. Many vertebrates have ears that function independently to receive pressure from incoming sound waves, determining directionality through neural processing and diffraction [3, 4]. Other animals, especially smaller ones, can take advantage of tympanal membranes coupled through shared bodies of air, converting their ears into pressure gradient receivers [3, 5]. However, as differences in received pressure and organismal length scales become smaller, this coupling strategy becomes less practical. And many invertebrates lack significant neural investment in central processing and rely heavily on mechanical structures to pre-process sensory signals [5–8].

The biophysics of sound localization for specific species is often too complex to be modeled easily. But a simple mathematical hearing model exists for the tachinid fly *Ormia ochracea* (*O. ochracea*). It can be used to extract key principles of binaural hearing without complex physiological modeling of neural processes.

For *O. ochracea*, the ability to hear its host plays a key role in its reproductive cycle and overall fitness. As a parasitoid, *O. ochracea* listens to chirping male crickets and follows the sound back to the source, where female *O. ochracea* then deposit their larvae [9]. Gravid *O. ochracea* females will remain in an area for extended periods in response to cricket chirping sounds, even if no cricket is present [10]. Given its small size, if *O. ochracea* relied exclusively on the distance between its prosternal tympanal membranes (figure 1(C)), the ITD it experienced would be at the nanosecond scale or below for the sound frequencies to which they are sensitive, and there would be no practical difference in sound amplitude between the two membranes (IAD). To solve this scaling problem without costly neurological investment, *O. ochracea* have two mechanically coupled membranous tympana directly beneath their head (figure 1(C)). These coupled tympana are composed of a pair of prosternal membranes, joined together by an intertympanal bridge [11], and are significantly larger in female *Ormia* (figure 1(C)). This distinctive mechanical coupling increases the ITD and IAD perceived by the fly. We will refer to the increased ITD and IAD as mITD and mIAD, respectively. These mechanically amplified values allow it to localize chirping crickets successfully. Since *O. ochracea* are active at or after dusk they also use their hearing to avoid predation by bats, exhibiting a startle response while in flight to bat sonar frequency sound, similar to praying mantises [12, 13]. Given *O. ochracea*'s ability to accurately and quickly locate a source of incoming sound at high levels of lateral angular resolution, even in potentially noisy environments [14], it may serve as a good source of bioinspiration to tackle the so-called cocktail party problem [15] (isolating sounds in a noisy environment) for directional microphones and hearing aids.

Accurate models of binaural hearing in animals are generally highly complex. Because of the mechanical nature of its acoustic sensing organ, *O. ochracea* is one of the few exceptions, and it has been the focus of numerous studies featuring its 'simple' hearing organs and how they function [11, 12, 16–22]. To investigate the biomechanical mechanisms that underlie *O. ochracea*'s unusual hearing abilities, Miles, Robert, and Hoy developed mechanical and mathematical models of the ormiine flies' coupled tympana in 1995 [18]. The authors validated their model against experimental data, recording tympanal membrane positions and velocities, and consequently mIAD and mITD, as a function of the incident sound pressure, intensity, and angle. The Miles model becomes analytically solvable under the assumptions of continuous sinusoidal input and symmetric model parameters, in addition to being numerically solvable without requiring the assumptions of symmetry or continuity. The model allowed Miles *et al* to demonstrate that *O. ochracea*'s impressive sound localization abilities are due to the pre-processing performed by their structurally coupled tympana, which mechanically amplifies the ITD and IAD experienced by the fly.

In addition to providing a physiological explanation for *O. ochracea*'s localization prowess, the Miles model also accurately predicted mITD for all incoming sound angles and mIAD for angles below $\pm 30°$ in a sample *O. ochracea* population. Both the measured

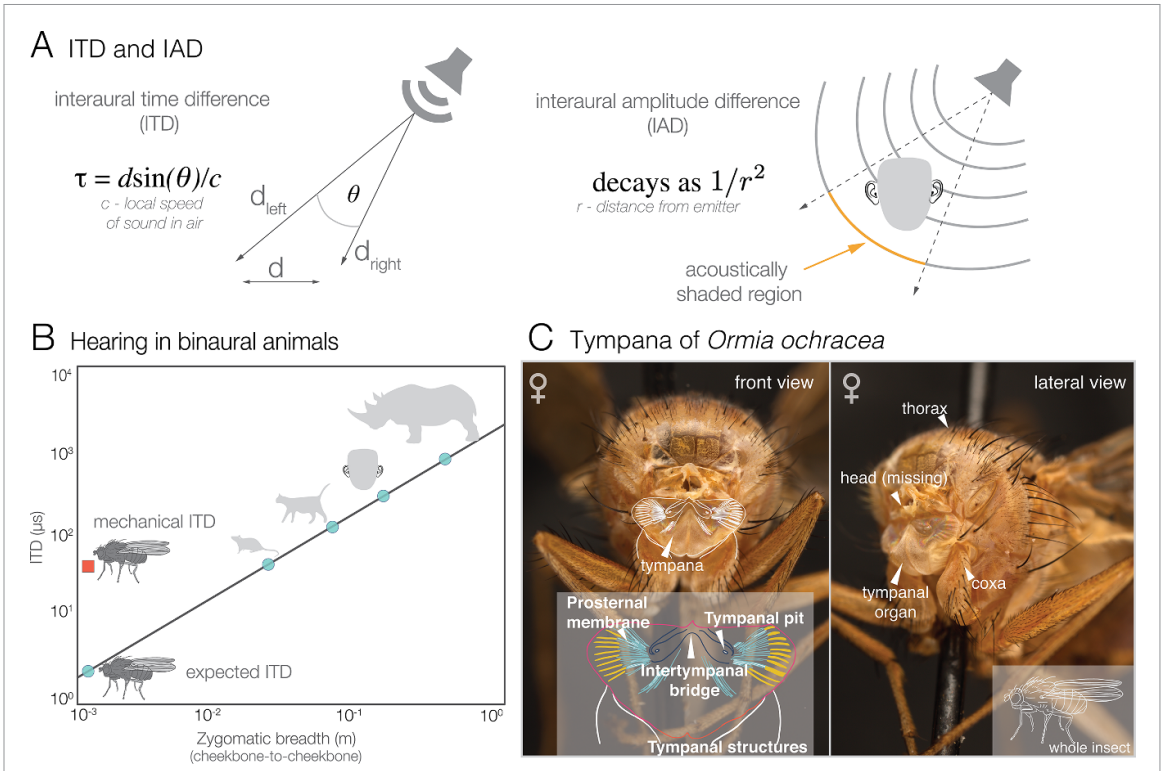

Figure 1. Hearing in binaural animals and the fly *Ormia ochracea*. (A) Physical meaning of ITD and IAD. ITD is the time delay between sound reaching one sensory organ relative to the other, defined by the equation $\tau = d\sin(\theta)/c$, where d is the distance between the hearing organs and c is the speed of sound in air. IAD is the difference in response amplitude between the left and right sensory organs, usually due to acoustic shading or signal decay. (B) Estimated ITD values in binaural animals of increasing size (*O. ochracea*, rat, cat, human, and rhinoceros) for a sound source at 45° from the midline, calculated using the formula in (A), with zygomatic breadth (cheekbone-to-cheekbone distance) used as a measure of interaural distance for mammals. The expected ITD for *O. ochracea* calculated based on intertympanal distance is indicated with a blue dot. The true value of ITD for *O. ochracea* is included as a red square ('mechanical ITD') to illustrate the degree of improvement in *O. ochracea*'s hearing acuity provided by its mechanically coupled tympana. Data for mammals from [32–35]. (C) Female *O. ochracea* post-decapitation, showing the location of the prosternal membrane, tympanal pits, and intertympanal bridge, key physical features in modeling its binaural hearing.

and predicted mITD indicated that *O. ochracea* possesses an mITD comparable to the ITD of an animal closer in size to a rat (figure 1(B)). Later experiments successfully determined that *O. ochracea* has a sound localization precision in the azimuthal plane of 2° [23, 24], comparable to that of humans. This high precision, together with the relative simplicity of the model and the easily reproducible structure of the hearing mechanism used by *O. ochracea,* led to a new stream of research in *O. ochracea*-inspired designs for directional microphones and hearing aids [25–31]. Despite its utility, the model contains a number of simplifications that limit its biological accuracy.

The Miles model is a lumped-element model that considers the dynamics of the intertympanal bridge and the tympanal membranes (figure 1(C)), modeling each membrane as a flat plate with a purely one-dimensional amplitude response. The tympana are represented as flat, front-facing membranes, though they lie on a convex surface at an angle from the flies' frontal and transverse planes. Miles *et al* adjusted the model's spring and damper coefficients until the model response approximated the experimental responses of the tympana in recently deceased *O. ochracea* specimens measured using laser vibrometry. Although the model is accurate for mITD in a narrow range of incident sound angles, it displays significant errors in mIAD for incident sound angles larger than approximately ±30° from the midline of the fly, and mITD becomes increasingly inaccurate at angles above approximately ±40°. This inaccuracy at large incident sound angles limits the model's power for explaining binaural hearing in *O. ochracea* and its potential for inspiring new hearing-based engineering.

In this work, we used three-dimensional (3D) reconstructions of the tympanal organs of two *O. ochracea* specimens, which we obtained via synchrotron x-ray imaging, together with the available behavioral hearing and tympanal response data, to identify candidate morphological features and possible additional mechanics not represented in the Miles model that could help explain the error in mITD predicted for large incident sound angles. While previous scanning electron microscopy images of *O. ochracea* tympana indicated that a degree of morphological

complexity was present [11], the 3D reconstructions allowed us to examine different views of the tympanal organ and form a more complete understanding of its structure.

Using the reconstructions as a guide, we identified the tympanal bridge arm angle, ϕ, which quantifies the tympanal membranes' relative orientation, and the angular width of the frontal tympanal organ segment between the membranes, as important to the perception of sound. We then modified the Miles model to include a differentiated mechanical response to incoming sound on the hearing organ's ipsi- and contralateral sides. These asymmetric parameter adjustments were represented mathematically via modified spring and damper coefficients that depend on the tympanal bridge angle, the frontal tympanal organ segment angle, and the incoming sound angle. Our model modifications were based on the hypothesized existence of unknown hearing mechanics akin to acoustic shadowing (which is not a feature of *O. ochracea*'s hearing mechanics at the host-cricket chirp frequencies that the flies' hearing system is tuned to perceive) that act to damp the response of the hearing organ on the contralateral side for certain incoming sound angles. We discuss the hypothesized mechanics further in this article's q2D model modifications, results, and discussion sections.

2. Materials and methods

2.1. Synchrotron x-ray imaging of the ormiine tympanal organ

To examine the 3D nature of *Ormia ochracea*'s tympanal morphology, we performed tomographic imaging of preserved *O. ochracea* specimens using synchrotron x-ray imaging at the Advanced Photon Source at Argonne National Laboratory. Two *O. ochracea* dried specimens were borrowed from the Virginia Tech Insect Collection. The specimens were placed in slender tubes made of polyimide, and the ventral thorax was imaged at beamline 2-BM using x-rays with an energy of 14 keV. Each specimen was imaged using the beamline's fast 2D phase-contrast imaging, giving stacks of images along the anterior–posterior-axis at intervals of 1.72 μm [43].

Reconstructed microtomographic images were cropped and down-sampled using FIJI [36], and segmented in SlicerMorph, [37] an imaging extension of 3D Slicer [38, 39]. To segment, features of the tympana were highlighted and then rendered in 3D for applicable measurements. The three-dimensional scans are available upon request.

2.2. Previous model

The previous model of binaural hearing in *O. ochracea* includes two components: a mechanical model of the anatomy and its function and a corresponding mathematical model. The mechanical model [18] treats the tympanal structure as a pair of beams pinned at a central pivot, with lumped-mass approximations of the two sides of the hearing organ located at the ends of the beams (figures 2(A) and (B)). The beams are anchored to the substrate at their distal ends with a pair of symmetric spring-damper elements and to each other with a third spring-damper element (figure 2(B)). Pressure forces from incident sound waves are applied to the point masses via a forcing function composed of the product of the incident pressure magnitude, the inward-facing unit normal vector, and the tympanal surface area, A (see the supplemental material for numerical values used in this study). A time delay is applied between the left and right sides based on the angle θ, which is the angle of the incoming sound wave relative to the midline of the fly, with 0° defined as straight ahead [18]. The time delay is calculated via the equation that appears in figure 1(A).

The mathematical model is a set of coupled ordinary differential equations representing the mechanical model's dynamics. It treats the incident acoustic pressure acting on the tympanal membranes as two point forces, $f_1(t)$ and $f_2(t)$, acting on the point masses representing the tympanal membranes and associated structures. The dependent variable in the problem is $\mathbf{x}(t)$, which represents the one-dimensional response of the tympana. The model can be written as follows:

$$\begin{bmatrix} k_1+k_3 & k_3 \\ k_3 & k_2+k_3 \end{bmatrix}\mathbf{x}+\begin{bmatrix} c_1+c_3 & c_3 \\ c_3 & c_2+c_3 \end{bmatrix}\dot{\mathbf{x}} + \begin{bmatrix} m & 0 \\ 0 & m \end{bmatrix}\ddot{\mathbf{x}}=\mathbf{f}, \tag{1.1}$$

$$\mathbf{f}=\begin{bmatrix} f(t) \\ f(t+\delta t) \end{bmatrix} \tag{1.2}$$

where $\mathbf{x}=(x_1(t),x_2(t))$ is the unknown response vector containing the vertical displacement of the left and rightmost tips of the beams in figure 2(B), which represent the two sides of the cuticular intertympanal bridge, the applied force is $\mathbf{f}=(f_1(t),f_2(t))$, and $\dot{(\,)}$ represents differentiation with respect to time, t. The parameters k_i and c_i are spring stiffness and damper constants, respectively, and the parameter m is the effective mass of all the moving parts of the auditory system [18].

2.3. Q2D model modifications based on ormiine morphology

The Miles model (equations (1.1) and (1.2)) consists of two coupled one-dimensional ordinary differential equations with time as the sole independent variable. In Miles *et al*'s analysis of their model, the ormiine hearing structure is assumed to be left–right symmetrical, and the spring and damper coefficients on the right and left sides are identical and constant for all incident sound angles, with

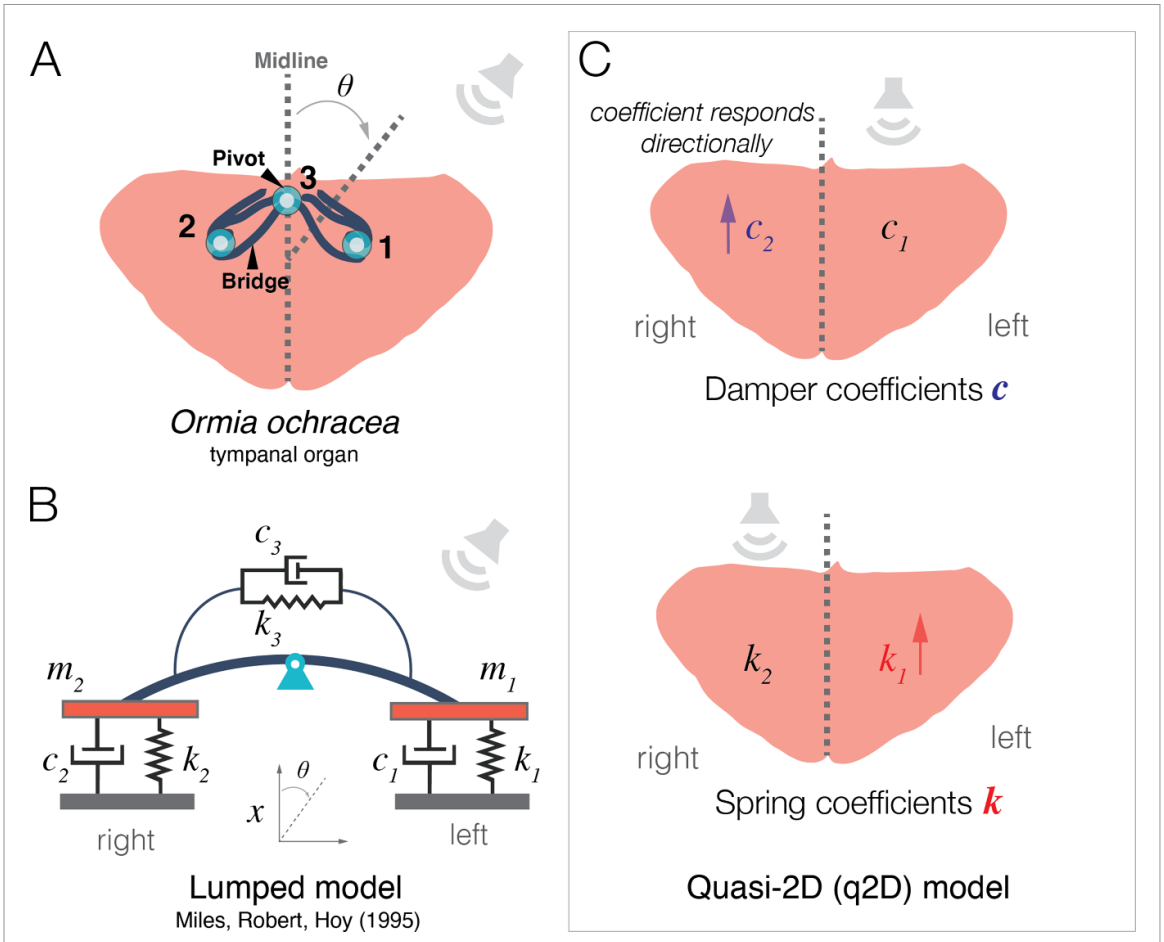

Figure 2. Modeling of binaural hearing in the fly *O. ochracea*. (A) Schematic of the coupled tympanal membranes of *O. ochracea* (peach-colored, labeled 1 and 2), connected by the cuticular intertympanal bridge (blue) with sound incident at $\theta°$. (B) The hearing system can be represented as a pair of coupled beams joined and anchored by a set of springs and dampers (Adapted with permission from [40]. Copyright © 2013, Springer Nature. CC BY-NC-ND 3.0) (C) The q2D model has an asymmetric response: the spring and damper coefficients on the contralateral (opposite) side from the sound source increase as a function of incident sound angle, while the coefficients on the ipsilateral side remain constant.

$k_1 = k_2 = k$ and $c_1 = c_2 = c$, independent of the values of k_3 and c_3. Although some sensitivity to the incoming sound angle θ is encoded in the Miles model via the time delay parameter, δt in equation (1.2), which is calculated according to the equation shown in figure 1(A), the model's predictions for mITD and mIAD are only accurate for small incoming sound angles (see figures 3(B) and (C)).

To add the level of sensitivity to the incoming sound angle represented in the available behavioral data, we modified the spring and damper parameters to incorporate aspects of the 3D morphology of the fly's hearing organ. The resulting model is quasi-two-dimensional (q2D) since it depends on the sound source's location in the azimuthal plane. Specifically, we treated the magnitude of the spring and damper coefficients, k and c, on the contralateral side as functions of the incoming sound angle for sounds incident between azimuthal angles approximately corresponding to sound arriving perpendicular to the ipsilateral membrane (θ_1) and sound arriving parallel to the contralateral membrane (θ_2). This variable response region corresponds to the yellow-shaded angle segment in figure 4(D). The functions were structured such that for incident sound angles above θ_1 (which is equivalent to $\phi - 90°$, where ϕ is the angular width of the frontal tympanal organ segment between the membranes), the k and c values corresponding to the contralateral tympanum are increased compared to those for the ipsilateral tympanum. This represents an overall damping of the contralateral tympanal response, or a stiffening of the contralateral tympanum. Our modified model posits three distinct tympanal response regimes: a symmetric regime in which incoming sound is incident near the front of the fly between the two tympana, and the tympana respond identically ($|\theta| \leqslant \theta_1$, the blue shaded region in figure 4(D)), a linear ramp regime in which the contralateral tympanum's response is damped and the damping increases as a linear function of the incoming sound angle ($\theta_1 \leqslant |\theta| \leqslant \theta_2$, the yellow shaded region in figure 4(D)), and a saturated regime in which the contralateral damping has reached a maximum level and no longer increases with incoming sound angle ($|\theta| \geqslant \theta_2$, the red shaded region in figure 4(D)).

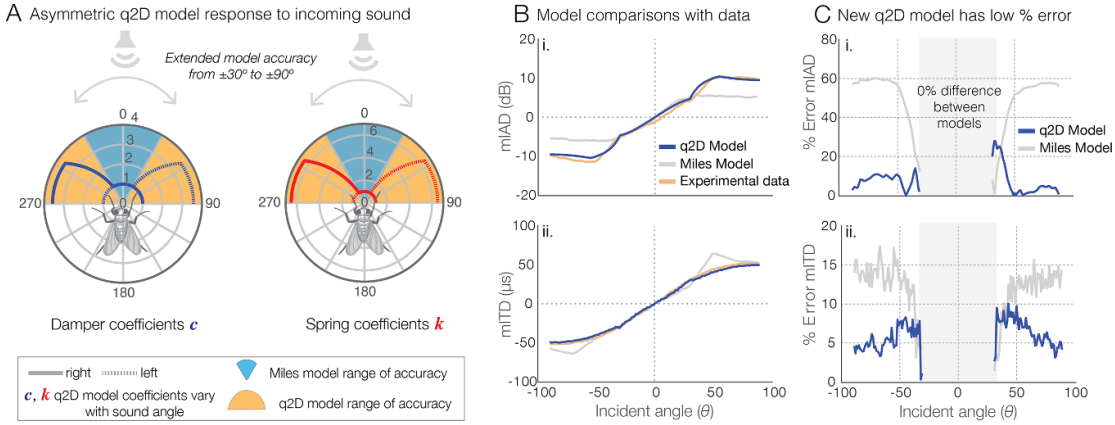

Figure 3. Model modifications and comparison between the Miles model, experimental data, and q2D model. (A) The modified q2D model shows improved range of accuracy in its response to incident sound. In the q2D model, the normalized damper (red) and spring (blue) coefficients are functions of the incoming sound angle. The improved q2D model responds accurately within $\pm 90°$, compared to $\pm 30°$ for the Miles model. Experimental and model results (B) and error (C) in mITD and mIAD for the standard one-dimensional (Miles model) and q2D models. In (B), mITD and mIAD were calculated from the q2D and Miles models as a function of incident sound angle for a frequency of 6,000 Hz and compared with laser-vibrometry measurements from recently deceased *O. ochracea* specimens provided in [18], as no other experimental data exists with which to compare our model's predictions. Data were obtained from [18] using the MATLAB program GRABIT [42] and the published PDF file, and the error for a given variable was calculated by finding the absolute value of the difference between the model results and the experimental data for that variable, dividing the difference by the experimental data value of the variable, and multiplying the result by 100. The significant divergence from behavioral data present in the Miles model outside $\pm 30°$, particularly for mIAD, is rectified in the modified q2D model. In (C), the gray box indicates errors below $\pm 30°$, which are not considered because the q2D and Miles models are identical for these ranges. The errors for the q2D model peak close to $\pm 30°$, then decrease as the incident sound angle increases.

This stiffening of the contralateral tympanum is due to unknown mechanics related to the structure of the tympanal organ that causes an asymmetric response to laterally oriented incoming sounds (figure 2(C)). This behavior would be consistent with the enhancement of directional hearing via a pressure gradient receiver mechanism resulting from internal acoustic coupling of the tympana, as in pyraloid moths [41] and many terrestrial vertebrates.

We provided the following q2D modification to the Miles model of ormiine hearing:

$$k(\theta) = \begin{cases} k_i & \text{if } |\theta| < \theta_1 \\ \alpha(|\theta| - \theta_1) + k_i & \text{if } \theta_2 > |\theta| \geqslant \theta_1 \\ k_f & \text{if } |\theta| \geqslant \theta_2 \end{cases} \quad (1.3)$$

$$\alpha = \left(\frac{k_f - k_i}{\phi - 90°} \right) \quad (1.4)$$

$$c(\theta) = \begin{cases} c_i & \text{if } |\theta| < \theta_1 \\ \beta(|\theta| - \theta_1) + c_i & \text{if } \theta_2 > |\theta| \geqslant \theta_1 \\ c_f & \text{if } |\theta| \geqslant \theta_2 \end{cases} \quad (1.5)$$

$$\beta = \left(\frac{c_f - c_i}{\phi - 90°} \right) \quad (1.6)$$

where k_i and k_f and c_i and c_f are the minimum and maximum values that the spring stiffness and damping coefficients take on, respectively, and ϕ is the intertympanal bridge arm angle (see figures 2(A) and 4(D)). The form of the modified spring coefficient function, two constant segments with a linear ramp between $\pm\theta_1$ and $\pm\theta_2$ (figures 2(C) and 3(A)), was also informed by the lateralization behavior observed in *O. ochracea* [23] and the analysis of an *O. ochracea*-inspired sensor [40]. These works indicated the presence of two separate behavioral regimes, a localization regime from 0° to 30° and a lateralization regime at higher angles. This choice is further supported by the accuracy of the fit to experimental data for sound incident at $\geqslant 30°$ (figures 3(B) and (C)), and physically represents a variable mechanical response to sound waves incoming laterally. These equations can be represented in a fully generalized form as:

$$d(\theta) = d_i(H(\theta_1 - \theta) + \delta_{\theta\theta_1}) + d_f(H(\theta - \theta_2) + \delta_{\theta\theta_2}) + \left(\left(\frac{d_f - d_i}{\phi - 90°} \right)(\theta - \theta_1) + d_i \right) H(\theta_2 - \theta) \times H(\theta - \theta_1) \quad (1.7)$$

where d, d_i, and d_f represent either the spring or damper coefficient and their start and end values respectively, δ_{ij} is the Kronecker delta function, and $H(i-j)$ is the Heaviside function. MATLAB's ODE45 function was used to integrate equations (1.1) and (1.2) for the Miles model and (1.1)–(1.6) for the modified q2D model. A custom peak-finding algorithm was implemented to calculate mITD and mIAD, which was necessary because of the asymmetry in the model coefficients k and c. Further computational details and a link to representative code samples can be found in [44].

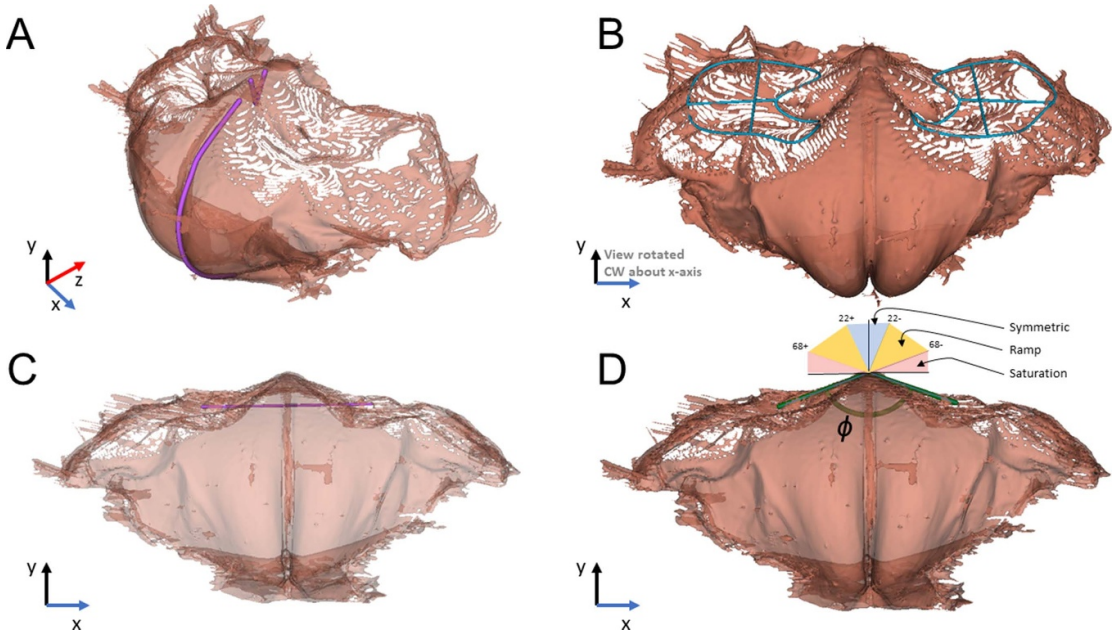

Figure 4. Main geometric features of *O. ochracea*'s tympanal organ. The *y*-axis points in the fly's forward-facing direction. (A) The curvature of the bottom arc of the prosternal inflation of the tympanal structure, the angle between the azimuthal plane and the bridge arms, and the total height of the arms are each indicated by purple line annotations. (B) The edges of the tympanal membranes are outlined in teal, and the width and depth of the membranes are indicated in teal. (C) The width of the tympanal bridge arms is indicated in purple. (D) The tympanal bridge arms and the angle between them, (ϕ), are indicated in dark green. The colored panel reflects the approximate symmetric, ramp, and saturation azimuthal response ranges of the modified q2D model tuned to this specimen. The q2D model regime bounding angles, θ_1 and θ_2 are 22° and 68°, respectively, for this specimen. See also movie S1 in supplemental information.

3. Results

The tympanal organ of *O. ochracea* protrudes anteriorly from underneath the fly's neck (cervix), with distinct lateral faces (prosternal tympanal membranes) and sharply angled intertympanal bridge arms (figure 5). The tympanal organ is a modification of the prosternum and is composed of a pair of front-facing (cephalad) tympanal membranes that cover a hollow prosternal cavity. The cavity opens to the environment through a pair of tracheae connected to lateral mesothoracic spiracles [11]. Each bridge arm has a pit that connects to an auditory apodeme that runs longitudinally through the sternal cavity to an auditory sensory organ (a bulba acustica, a chordotonal organ composed of many sensory scolopidia). Vibrations are conducted via the apodemes to the bulbae acusticae, which are innervated to the frontal nerve of the thoracic ganglion.

Figure 5 shows 3D surface renderings of *O. ochracea* tympanal membranes in teal, with the supporting sternal structures highlighted in peach. The organs are far from the simple two-dimensional surfaces most often depicted in the literature [17, 18, 31, 40]. These new 3D models motivated our modifications to include aspects of actual morphology. The confirmation of significant bilateral faces of the tympanal organ led to the modifications present in the q2D model (equations (1.3)–(1.6)), which account for the lateral tympanal organs' response to acoustic stimuli. Because the specimens are preserved, some aspects of the morphology, especially the degree of bowl-like curvature of tympanal membranes visible in figure 5, may be due at least partially to the desiccation of the samples. However, the overall topography of the structures, especially the tympanal bridge, appears to remain essentially unchanged when compared to previous still images taken of recently sacrificed specimens [18].

Using the 3D renderings, we measured several features of *Ormia* tympanal morphology, as shown in figures 4(A)–(D). Because the rendering is produced using images sampled every 1.72 μm, features smaller than this may not be visible.

In figure 4(A), the prosternal inflation of the tympanal structure is traced in purple. The path length and curvature of the tracing were measured. The mean curvature is 0.004 μm^{-1}, and the maximum curvature is 0.018 μm^{-1}, highlighting the presence of extended flat portions of the supporting structure. The plane of the intertympanal bridge arms (shown in purple) is oriented upwards relative to the azimuthal (x–y) plane by 38°. The vertical height of the connecting line between the horizontal span of the intertympanal arms and the point at which they join, in the y direction (also shown in purple), is

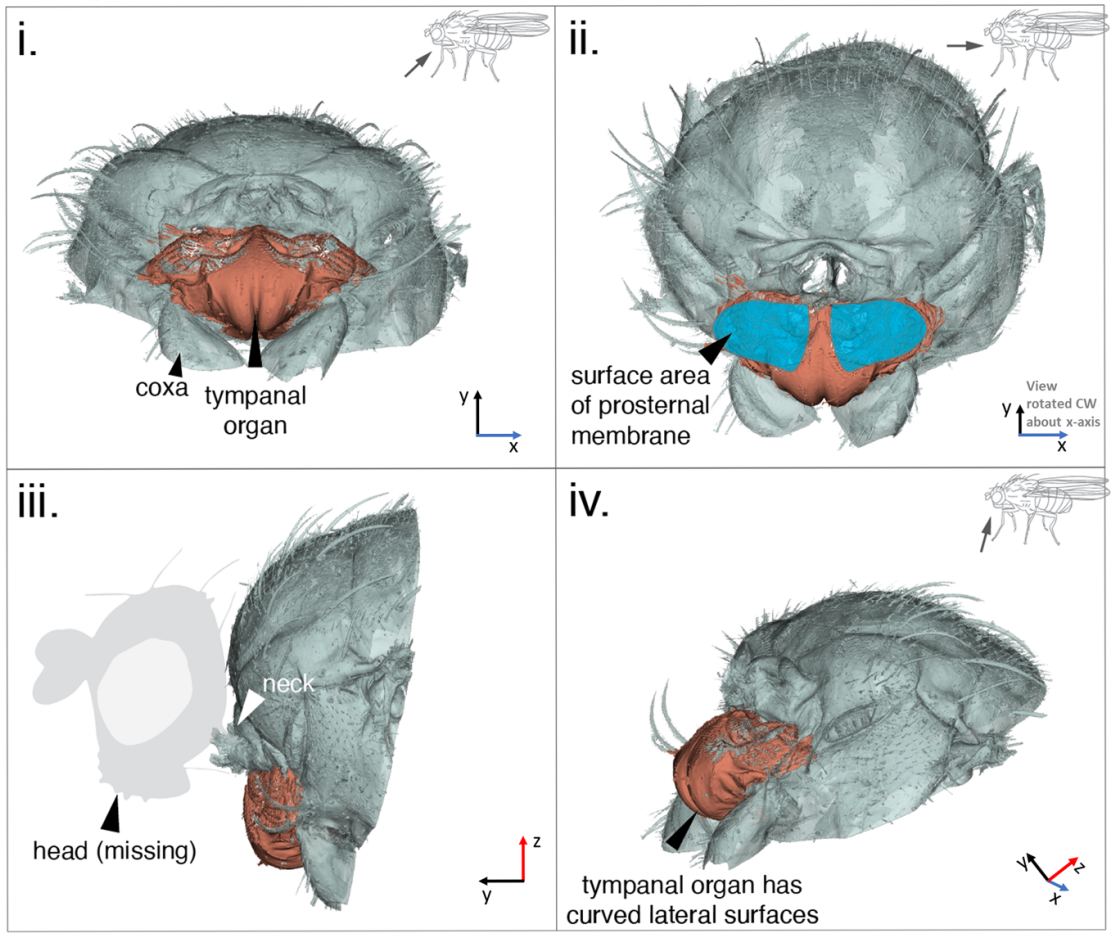

Figure 5. 3D rendering of tympanal organs and frontal prothorax of the fly *Ormia ochracea*. The tympanal membranes are highlighted in blue (ii.), and the supporting structures are highlighted in peach. The view directions are indicated in schematics at the top right of the images. 3D images made in SlicerMorph software [37].

73 μm. In figure 4(B), the boundaries of the tympanal membranes are outlined in teal. The outlines of the membranes are approximately oval, with a mean curvature of 0.011 μm^{-1} and 0.0012 μm^{-1} for the left and right membranes, respectively. The membrane tracings were measured to have an approximate surface area of 0.647×10^{-6} and 0.656×10^{-6} m^2 for the right and left membranes, respectively, with corresponding width and depth values of 207 μm and 226 μm, and 229 μm and 249 μm. Figure 4(C) shows the horizontal (x-axis) span of the bridge arms, joined by the purple line, which is measured to be 405 μm.

Figure 4(D) outlines the tympanal bridge arms in dark green. The length of the outline of the right arm is 222 μm, and the outline of the left arm is 214 μm. The angle between the two is 136.2°.

As discussed in the q2D model modifications section, careful inspection of the 3D renderings led us to hypothesize that including a representation of the orientation of the tympanal membranes and the angular distance between their front edges in the mathematical model would improve its performance. This improvement was hypothesized because the membranes' relative orientation appears to be related to the angles at which the flies' tympanal responses changed in experimental studies. In the updated q2D model, the contralateral tympanum's response is damped for incoming sound first incident at locations between the front edge and the center of the ipsilateral tympanal membrane. Because acoustic shading is not possible for the frequencies to which the flies are sensitive, one reasonable explanation is a previously unidentified mechanical feature causing angle dependence in the tympanal organ's response, as discussed in the model modifications section above.

The arms form an angle ϕ of approximately 136° within the azimuthal plane, which creates a 112° angle with the midline of the fly. Therefore, sound incoming at a 22° angle (relative to the y-axis or midline in figure 3(D)) would be oriented perpendicular to the ipsilateral arm, indicating the beginning of an incoming sound angle regime in which the contralateral tympanal membrane exhibits increasingly damped responses. Similarly, incoming sound at a

68° angle from the midline would be parallel to the contralateral arm, corresponding to maximal damping of the contralateral membrane.

Hence, 22° and 68° from this specimen's midline (y-axis) represent incoming sound angles that divide the three hypothesized tympanal response regimes introduced in the q2D model modifications section: symmetric, linear ramp, and saturated. In the symmetric regime ($|\theta| < 22°$), the tympana will respond symmetrically. In this regime, the model coefficients k_i and c_i are constant. In the linear ramp regime ($22° < |\theta| < 68°$), both tympanal membranes will vibrate in response to incoming sound in a ratio that depends on θ, and the model coefficients vary linearly as described in equations (1.3)–(1.6). In the saturated regime, the contralateral tympanal membrane's damper and spring coefficients will have reached their maximum values, c_f and k_f. The coefficients will be constant in this regime. This trimodal behavior appears to be due to unidentified mechanics of the tympanal organ that are seemingly well-modeled by increasing damping of the contralateral membrane in response to increasing incoming sound angles in the specified range.

We used the values $\theta_1 = 30°$ and $\theta_2 = 55°$ in our modified q2D model to obtain the q2D model results shown in figures 3–7. These values are tuned to match the available behavioral data from [18], shown in figure 3(B) (mITD and mIAD values derived from laser-vibrometry measurements of tympanal membrane displacements in *O. ochracea* specimens in response to a 6 kHz sound source, as a function of incident sound angle). We assumed the total tympanal surface area, A, was fixed and used the value from [18] ($A = 0.288 \times 10^{-6}\,\mathrm{m}^2$). The increases in the spring and damper coefficients, normalized relative to their nominal values (k_i), are visible in figure 4(A). The values for θ_1 and θ_2 used in our computations differ from the angles that bound the ramp regime represented on the fly in figure 4(D) (shaded yellow). This is because we used 3D imaging of the fly in figure 4 to identify the geometric features of *O. ochracea*'s hearing organ that are important for sound localization. While the importance of these features generalizes to all *O. ochracea* individuals, the exact value of the intertympanal bridge arm angle, ϕ, is subject-specific. We expect that if we had behavioral data for the fly imaged in figure 4, the values of the modified model's ramp regime bounding angles that provided the best match to that data would be ±22° and ±68°, as shown in figure 4(D).

Values of mITD and mIAD, calculated from the q2D and Miles models, are shown in figure 3(B) as a function of incident sound angle and are compared to experimental measurements in recently sacrificed *O. ochracea* specimens [18]. Both models are identical for incident sound angles less than ±30°, so the results are identical within that range (figure 3(C), gray box). When we included the differentiated lateral response through the new $k(\theta)$ and $c(\theta)$ functions in equations (1.3)–(1.6), the gap between experimental measurements and model results in both mIAD and mITD narrowed significantly for 6 kHz signal input (figures 3(B) and (C)), with the q2D model having an average error of approximately 6% and a peak error of approximately 28% in mITD, and an average error of approximately 7% and a peak error of approximately 10% in mIAD. These results additionally confirm that aspects of mechanics in two dimensions are important elements of ormiine hearing.

The model behaviors outside of the regime associated with cricket calls (roughly 4–6 kHz) were also examined and are shown in figures 6 and 7. These results demonstrate that, as a general rule, mITD values from both models approach zero as the frequency of incoming sound increases beyond 20–30 kHz. The sensitivity in mITD to the angle of incoming sound also decreases. There are small asymmetric regions in our q2D model, one from approximately 45° to 75° and 20 to 30 kHz, and one from approximately −15° to 0° and 0 to 10 kHz (figure 6(B)). Because the region where $|\theta| \leqslant 30°$ should be identical between the Miles model and the q2D model, with no asymmetry present, these asymmetries are likely numerical artifacts related to the peak-finding algorithm we used to determine mITD. This asymmetry is not present in the mIAD results (figure 7), nor in the divergence from the Miles model within the ±30° range, further supporting its characterization as a numerical artifact.

By contrast, figure 7 demonstrates that mIAD values are significant for all frequencies and angles well into the range of expected bat ultrasonic calls, especially in the q2D model. The angular resolution of mIAD (that is, the change in mIAD as the incoming sound angle changes by a fixed amount) decreases with incoming sound angle for high frequencies, but this difference is consistent with observed *Ormia* behaviors that indicate that behavioral responses are tied more directly to successful bat identification, and less to precise localization [12] of the origin of ultrasonic bat vocalizations.

Additional figures showing independent left/right membrane response curves at specific incoming sound angles, as well as versions of figures 6 and 7, focused on the range from 1 to 20 kHz are available in the appendix. It should also be noted that above approximately 10 kHz in figure 6, the sign of the mITD values provided by both models shifts, indicating the contralateral response occurs prior to the ipsilateral response at high frequencies. This sign change and differences in mIAD signal values at high frequencies could provide an effective categorization mechanism for bat-signal and cricket-signal perception, as well as basic localization abilities into the ultrasonic frequencies for incoming sound, as was proposed in [12].

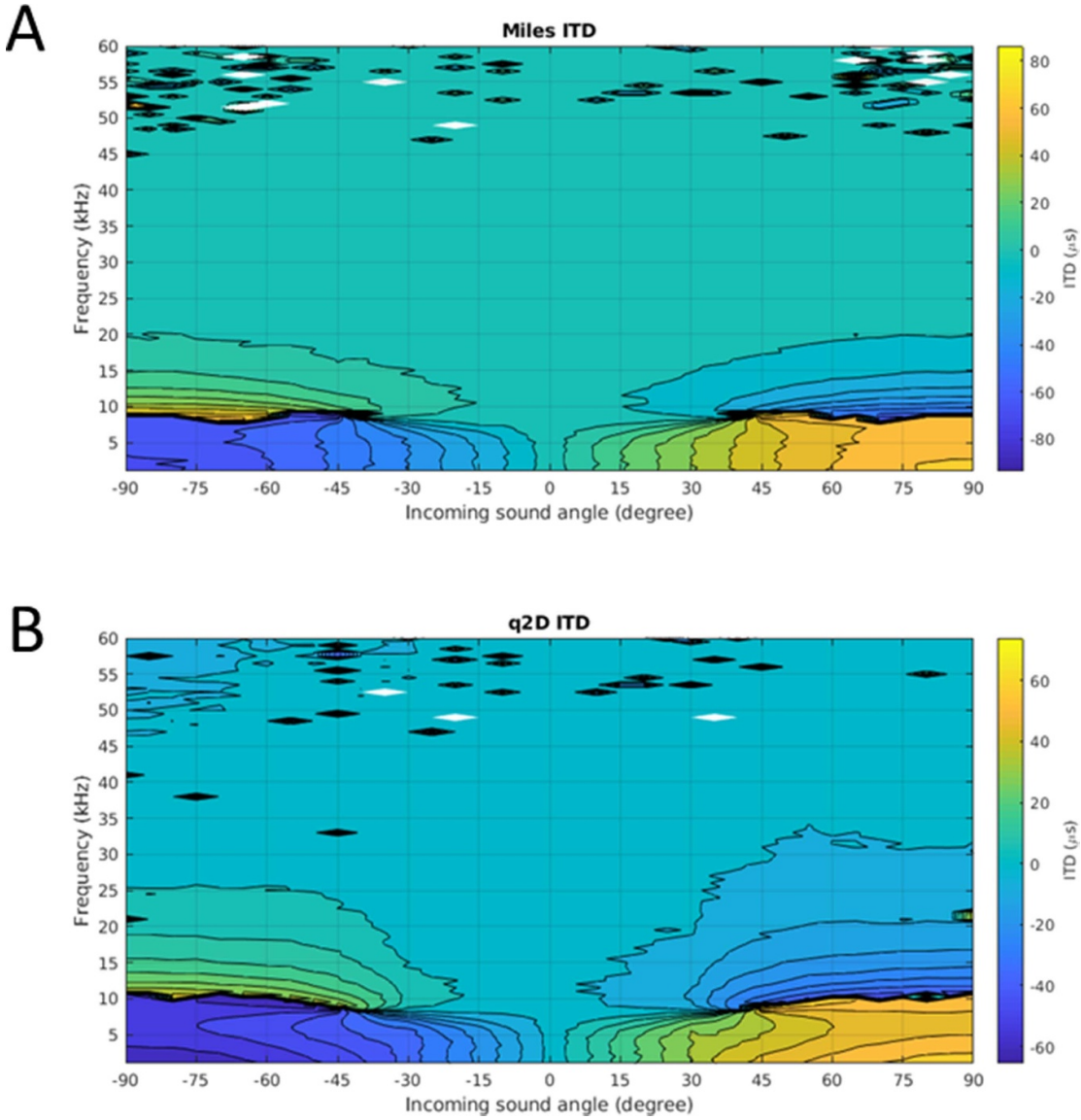

Figure 6. Model comparison at extended frequencies: mITD. The system mITD responses between the two tympanal membranes at incoming sound angles ranging from −90° to 90°, and frequencies ranging from 1 kHz to 60 kHz are shown for the Miles model (A) and the q2D model (B). mITD values approach zero above approximately 20 kHz in the Miles model (A) and 35 kHz in the q2D model (B). mITD values are highest at high incoming sound angles. White spots on the plot represent elements that were measured incorrectly due to erroneous identification in the peak finding algorithm used to determine mITD values.

4. Discussion

This paper presents the results of 3D x-ray synchrotron imaging of the mechanically-coupled tympana in the parasitoid fly, *O. ochracea*, and our subsequent modification to the classic mathematical model of hearing in *O. ochracea*, which was informed by those imaging studies. Three geometric features of the tympanal organ were identified as particularly important for sound localization: the angle ϕ between the inter-tympanal bridge arms, the angle θ_1, which is equivalent to $90° - \phi$, and the angle θ_2, which is half the azimuthal angle segment at the center of the fly, between the two tympanal membranes (see figure 4(D)). Thus, the convexity of the tympanal organ is represented in our modified model, in contrast to previous simplified representations of *Ormia ochracea*'s tympana as being located in a common frontal plane of the fly, level with the peak of the tympanal bridge.

Detailed knowledge of the hearing organ's morphology allowed us to update the classic one-dimensional mathematical model (the Miles model) into a quasi-two-dimensional (q2D) model of ormiine hearing that mimics the tympanal organ response in the lateral direction. Our updated q2D model has significantly improved agreement with available experimental data [18] compared to the Miles model, both in the mITD and in the mechanical mIAD (figures 3(B) and (C)). Compared to the Miles model, the new q2D model exhibits a reduction in maximum errors (relative to experimental values) of approximately 50% and 85% in mITD and mIAD, respectively. This result supports the premise that there are essential aspects of the mechanics of *Ormia* hearing aside

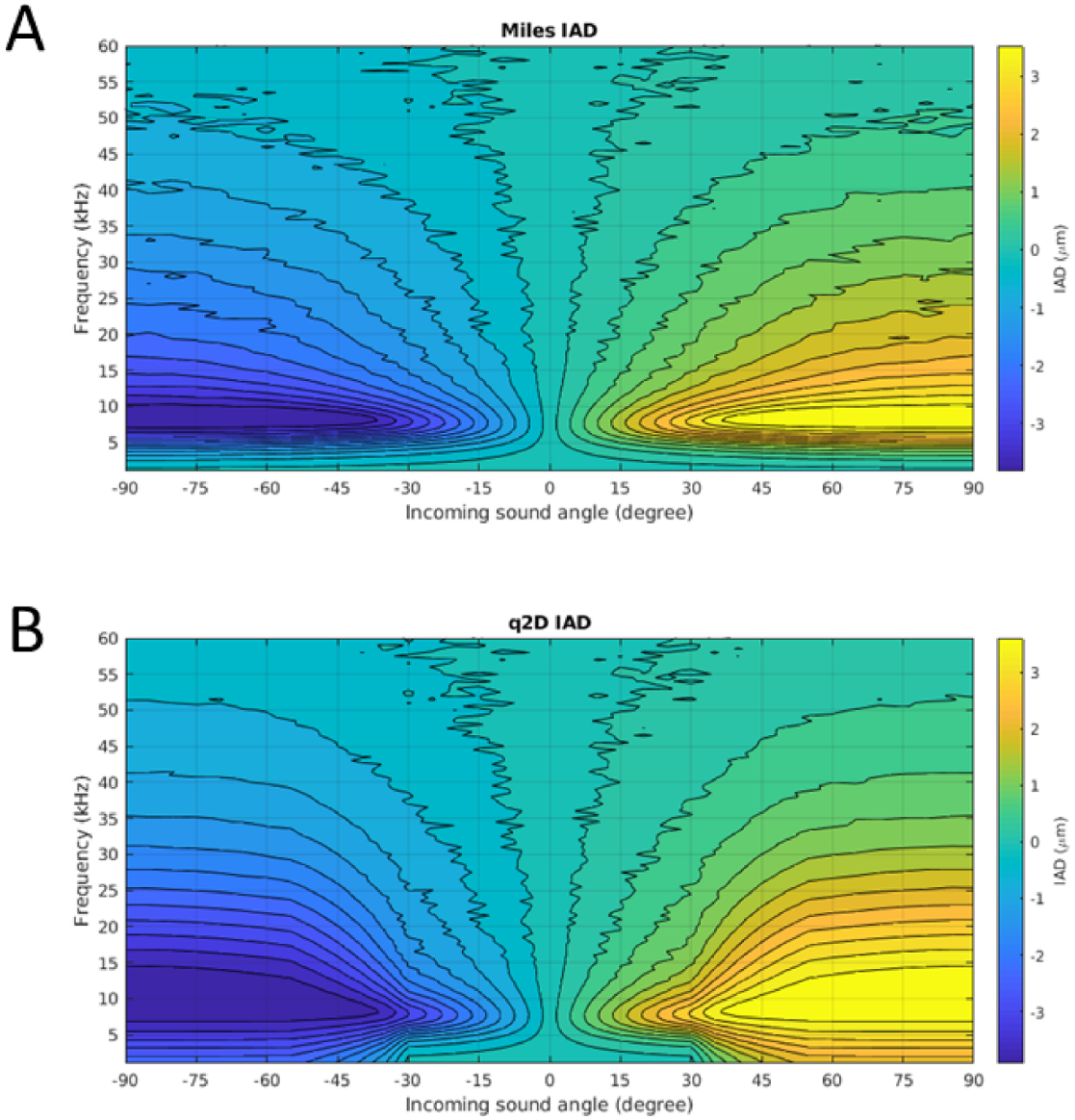

Figure 7. Model comparison at extended frequencies: mIAD. The system response amplitude difference (IAD) between the tympanal membranes at incoming sound angles ranging from −90° to 90°, and frequencies ranging from 1 kHz to 60 kHz are shown for the Miles model (A) and the q2D model (B). Unlike for mITD, non-zero mIAD values persist up to 60 kHz, the highest incoming sound frequency simulated. In both models, mIAD values are the highest at high incoming sound angles, with steeper value gradients occurring at lower frequencies, closer to the values expected values for cricket calls. The range of peak mIAD values (dark blue/bright yellow) is taller for the q2D model and extends into the low ultrasonic range.

from the uniplanar response of the tympanal membranes and that the hearing organ structures are sensitive to the angle of incoming sound, a feature that was not included in the Miles model.

Prior to our study, the original Miles model was the only existing model of internally coupled ears-based hearing in ormiine flies [45]. This is one of the first attempts to update the foundational Miles model for hearing in *O. ochracea*. Our model may be further refined by incorporating additional mechanical behaviors of the tympana, such as tympanal deflection in the lateral direction or a representation of the tympanal response in the vertical direction. Simple analytic modifications could also improve and expand the model's capabilities without impacting its tractability, such as using functions that are more flexible than simple linear ramps for the spring and damper coefficients. For example, in our q2D model, the 'bump' visible near ±45° in mIAD in figure 3(B) and the uptick at the same point in mITD may be a result of the values for either the springs, dampers, or the ratio between the two, being slightly too high at that point. It is also important to note that this work and the Miles model both rely on tuning the coefficients so that the model outputs better match the experimental response to sinusoidal input (2 kHz for the original 1995 work and 6 kHz for the work here). Although the q2D model's performance was not observed to degrade (compared to the original model) at other frequencies that we checked, the

degree of improvement (relative to the 6 kHz experimental data) was far less significant for other frequencies. The model's reduced performance at frequencies other than those tuned specifically for crickets could potentially be resolved by introducing other morphological features in the form of frequency-dependent functions in a similar way as we have introduced spatially-dependent functions here.

In the larger context of bidirectional mechanically-coupled hearing, this model provides an alternate pathway for exploring possible frameworks for mechanically-coupled ears. Many existing models of coupled hearing focus on the coupling mechanism itself and do not consider the orientation of incoming sound when determining the properties of the mechanism [3, 4, 46]. While the particular mechanism used by *Ormia* is unlikely to be replicated in other systems without similar mechanical coupling, the work presented here demonstrates the importance of the sensitivity of some microscale mechanical structures to the direction of incoming acoustic forces. It also underscores some shortcomings inherent to model simplification and motivates the development of models that, while remaining tractable, employ slightly more sensitive approaches.

Our model demonstrates a potential role for detailed tympanal anatomy in the mechanics and modeling of directional hearing in *O. ochracea*, especially with respect to the values of mIAD in response to incoming sound waves at high angles. Including angle-dependent behavior in the spring and damper coefficients may provide a more accurate representation of how the insect receives sound. Previous work has demonstrated that *O. ochracea* engages in different behaviors depending on the relative angle of incoming sound [18, 23, 40, 47], with two distinct response patterns. In the first, from 0° to ±30°, the fly makes relatively narrow adjustments to localize the origin of the sound (localization). In the other, at angles exceeding approximately ±30°, the fly makes more significant positional adjustments, more akin to determining the side from which the sound originates (lateralization). Our results suggest that angle-dependent tympanal membrane mechanics could contribute to this observed behavioral sensitivity to incoming sound angle.

There is growing evidence that some *O. ochracea* are involved in an evolutionary arms race with their host species [48, 49], and that they are capable of differentiating between different cricket host species based on their acoustic signaling, exhibiting preference towards local populations [50]. Consequently, the mechanical parameters for the model may depend not only on the geographic origin of *O. ochracea* samples, but also when collection occurred. The degree of tuning to host-searching behavior, as opposed to predator-avoidance behavior, also remains unaddressed experimentally, despite the startle responses when in flight and subjected to sound consistent with bat sonar frequencies [12]. *O. ochracea* exhibits a sorting behavior (being able to rapidly categorize sounds as belonging to a predator or not) in response to predator-consistent sound sources, as opposed to host or neutral sound sources [12]. *O. ochracea* is also only one of many *Ormia* species, which parasitize a diverse range of hosts, and display different behavioral responses to the acoustic signaling of their hosts [10]. Only *O. ochracea* has been examined in sufficient detail to develop a mechanical model with accurate parameters; consequently, it may be worth investigating the mechanics of other ormiine species [10, 51] and developing mechanical models similar to the q2D model presented here. It may also be worth revisiting the hearing organs in *Emblemasoma*, another group of parasitoid flies representing a case of convergent evolution in a distantly related family, Sarcophagidae [52, 53].

O. ochracea's hearing system has repeatedly been a source of inspiration for bio-inspired designs for directional microphones and hearing aids [25–31, 40]. Including the angle-dependent behavior of the expanded q2D model in future *Ormia*-inspired device designs may also provide significant avenues for improvement in device performance or may expand the functionality of devices like acoustic sensors through miniaturization and tunable frequency sensitivities. Currently, work is being undertaken to explore the inclusion of lateral faces on a directional microphone to study these elements' role further and attempt to develop a novel practical application. However, there are numerous avenues for exploration remaining, both experimental and theoretical. These include the development of improved bio-inspired technology by incorporating higher-dimensional features and parameter variations in the mechanical system, studying the model's behavior at frequencies commensurate with bat sonar, and investigating the role mechanical differences play in *O. ochracea*'s hearing when addressing acoustic preferences.

Finally, our expanded q2D model is the first mathematical model of hearing in a binaural fly that is accurate for all measured incident sound angles. It demonstrates the importance of incorporating higher-dimensional model elements consistent with observed physiology to further our understanding of binaural and insect hearing.

Data availability statements

The data that support the findings of this study are openly available at the following URL/DOI: https://github.com/aestaples/Ormia3D.

Acknowledgments

The authors thank the Virginia Tech Insect Collection for lending the *Ormia ochracea* samples for imaging, and Pavel Shevchenko for assistance in imaging at 2-BM at Argonne National Laboratory. The use of the APS was supported by the US Department of Energy, Office of Science, Office of Basic Energy Sciences, under Contract DE-AC02-06CH11357.

Author contributions

M R M-S developed the modified model; M R M-S and A E S designed and wrote the code; M K S and J J S performed 3D imaging data collection and analysis; M R M-S produced the hearing model data; M R M-S and A E S analyzed the hearing model data; M R M-S and M K S made the figures; P E M performed photographic work; M R M-S wrote the paper, and M R M-S, M K S, A E S, J J S, and P E M edited the paper.

Conflict of interest

The authors declare no conflict of interest. The funders had no role in the design of the study; in the collection, analyses, or interpretation of data; in the writing of the manuscript, or in the decision to publish the results.

Funding

This material is based upon work supported by the National Science Foundation under Grant Nos. 2014181, 1812215, 1437387, and 0938047.

Appendix

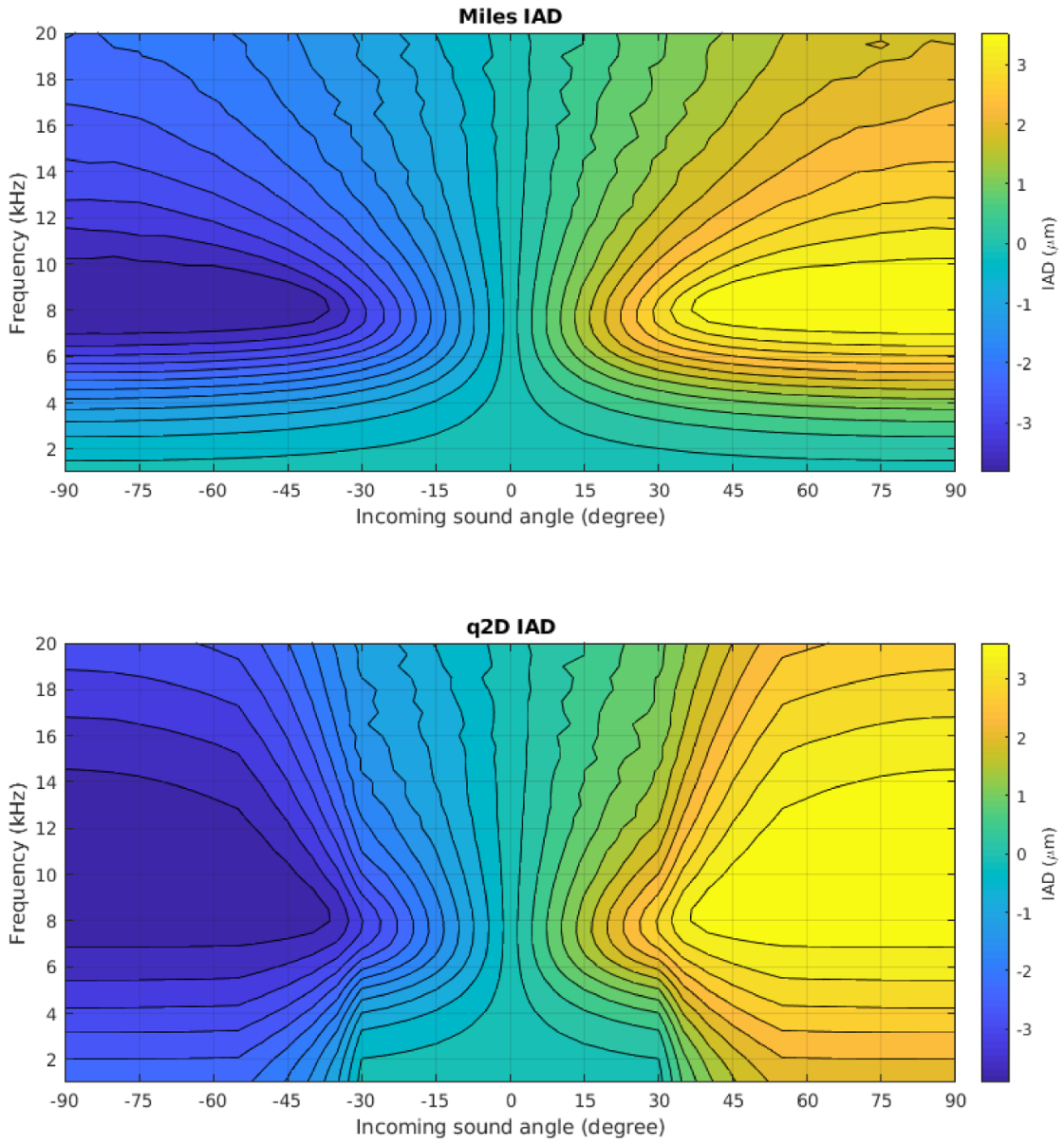

Figure 8. Model comparison at extended frequencies: mIAD (limited range). A limited (1–20 kHz) range view of figure 7.

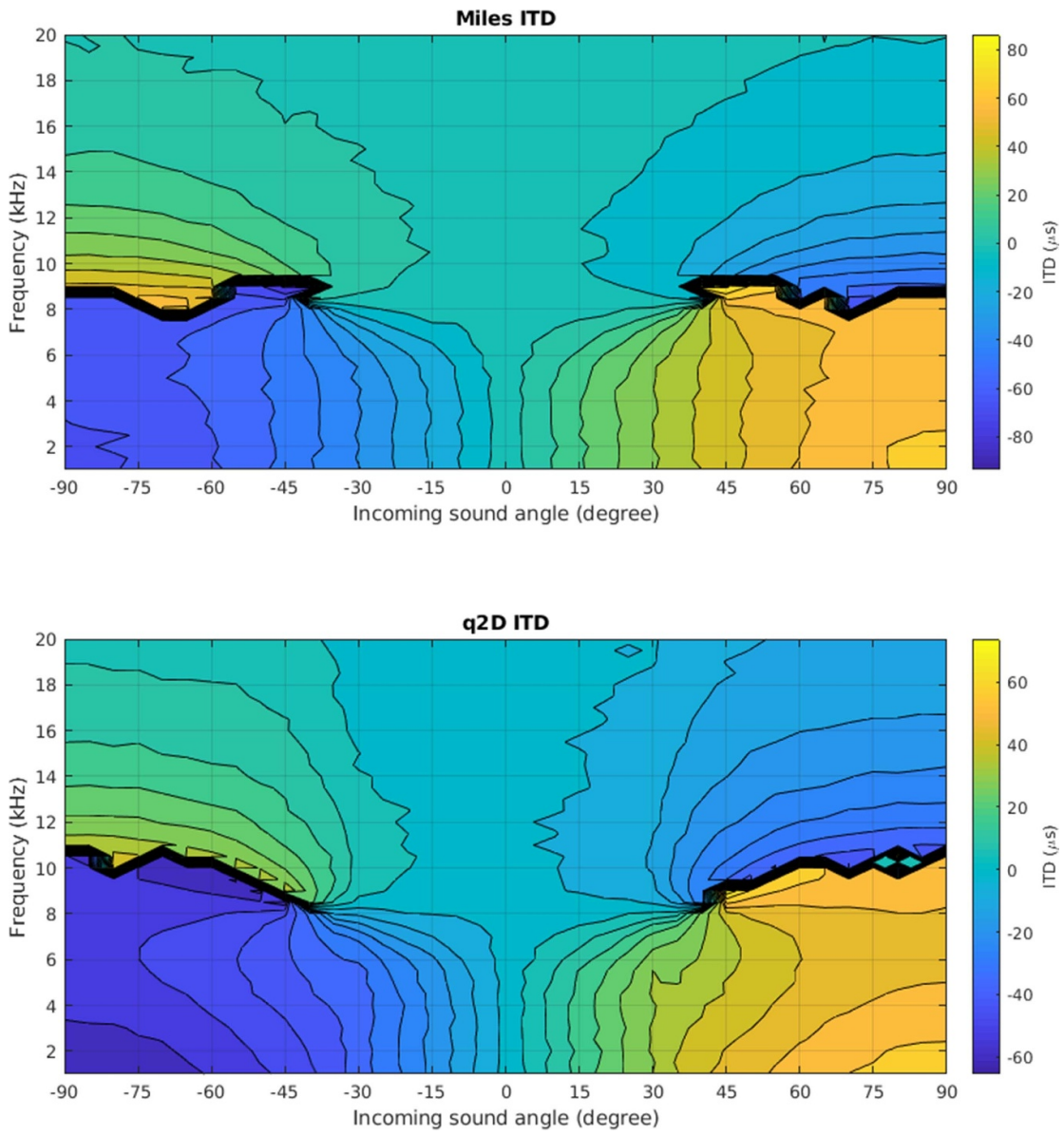

Figure 9. Model comparison at extended frequencies: mITD (limited range). A limited (1–20 kHz) range view of figure 6.

ORCID iDs

Max R Mikel-Stites https://orcid.org/0000-0002-4574-1414
John J Socha https://orcid.org/0000-0002-4465-1097
Paul E Marek https://orcid.org/0000-0002-7048-2514
Anne E Staples https://orcid.org/0000-0003-4823-8184

References

[1] Lord Rayleigh L 1907 XII. On our perception of sound direction *London, Edinburgh Dublin Phil. Mag. J. Sci.* **13** 214–32
[2] Jeffress L A 1948 A place theory of sound localization *J. Comp. Physiol. Psychol.* **41** 35
[3] Christensen-Dalsgaard J and Manley G A 2008 Acoustical coupling of lizard eardrums *J. Assoc. Res. Otolaryngol.* **9** 407–16
[4] Fletcher N H and Thwaites S 1979 Physical models for the analysis of acoustical systems in biology *Q. Rev. Biophys.* **12** 25–65
[5] Römer H 2020 Directional hearing in insects: biophysical, physiological and ecological challenges *J. Exp. Biol.* **223** jeb203224
[6] Menda G, Nitzany E I, Shamble P S, Wells A, Harrington L C, Miles R N and Hoy R R 2019 The long and short of hearing in the mosquito *Aedes aegypti Curr. Biol.* **29** 709–14
[7] Windmill J F C, Jackson J C, Tuck E J and Robert D 2006 Keeping up with bats: dynamic auditory tuning in a moth *Curr. Biol.* **16** 2418–23
[8] Brownell P and Farley R D 1979 Detection of vibrations in sand by tarsal sense organs of the nocturnal scorpion, *Paruroctonus mesaensis J. Comp. Physiol.* **131** 23–30
[9] Cade W H 1975 Acoustically orienting parasitoids: fly phonotaxis to cricket song *Science* **190** 1312–3

[10] Walker T J 1993 Phonotaxis in female *Ormia ochracea* (Diptera: Tachinidae), a parasitoid of field crickets *J. Insect Behav.* **6** 389–410
[11] Robert D, Read M and Hoy R 1994 The tympanal hearing organ of the parasitoid fly *Ormia ochracea* (Diptera, Tachinidae, Ormiini) *Cell Tissue Res.* **275** 63–78
[12] Rosen M, Levin E C and Hoy R R 2009 The cost of assuming the life history of a host: acoustic startle in the parasitoid fly *Ormia ochracea J. Exp. Biol.* **212** 4056–64
[13] Yager D D 2012 Predator detection and evasion by flying insects *Curr. Opin. Neurobiol.* **22** 201–7
[14] Lee N, Elias D O and Mason A C 2009 A precedence effect resolves phantom sound source illusions in the parasitoid fly *Ormia ochracea Proc. Natl Acad. Sci.* **106** 6357–62
[15] Bee M A and Micheyl C 2008 The cocktail party problem: what is it? How can it be solved? And why should animal behaviorists study it? *J. Comp. Psychol.* **122** 235
[16] Robert D, Amoroso J and Hoy R R 1992 The evolutionary convergence of hearing in a parasitoid fly and its cricket host *Science* **258** 1135–7
[17] Akcakaya M and Nehorai A 2008 Performance analysis of the *Ormia ochracea*'s coupled ears *J. Acoust. Soc. Am.* **124** 2100–5
[18] Miles R N, Robert D and Hoy R R 1995 Mechanically coupled ears for directional hearing in the parasitoid fly *Ormia ochracea J. Acoust. Soc. Am.* **98** 3059–70
[19] Cade W H, Ciceran M and Murray A-M 1996 Temporal patterns of parasitoid fly(*Ormia ochracea*) attraction to field cricket song (gryllus integer) *Can. J. Zool.* **74** 393–5
[20] Robert D, Miles R N and Hoy R 1998 Tympanal mechanics in the parasitoid fly *Ormia ochracea*: intertympanal coupling during mechanical vibration *J. Comp. Physiol.* A **183** 443–52
[21] Robert D and Willi U 2000 The histological architecture of the auditory organs in the parasitoid fly *Ormia ochracea Cell Tissue Res.* **301** 447–57
[22] Oshinsky M L and Hoy R R 2002 Physiology of the auditory afferents in an acoustic parasitoid fly *J. Neurosci.* **22** 7254–63
[23] Mason A C, Oshinsky M L and Hoy R R 2001 Hyperacute directional hearing in a microscale auditory system *Nature* **410** 686–90
[24] Mason A C, Lee N and Oshinsky M L 2005 The start of phonotactic walking in the fly *Ormia ochracea*: a kinematic study *J. Exp. Biol.* **208** 4699–708
[25] Miles R N and Hoy R 2006 The development of a biologically-inspired directional microphone for hearing aids *Audiol. Neurotol.* **11** 86–94
[26] Bauer R, Zhang Y, Jackson J C, Whitmer W M, Brimijoin W O, Akeroyd M A, Uttamchandani D and Windmill J F C 2017 Influence of microphone housing on the directional response of piezoelectric mems microphones inspired by *Ormia ochracea IEEE Sens. J.* **17** 5529–36
[27] Zhang Y, Bauer R, Jackson J C, Whitmer W M, Windmill J F C and Uttamchandani D 2018 A low-frequency dual-band operational microphone mimicking the hearing property of *Ormia ochracea J. Microelectromech. Syst.* **27** 667–76
[28] Touse M, Sinibaldi J and Karunasiri G 2010 MEMS directional sound sensor with simultaneous detection of two frequency bands *Sensors, 2010 IEEE* (IEEE) pp 2422–5
[29] Gibbons C and Miles R N 2000 Design of a biomimetic directional microphone diaphragm *Proc. IMECE* (ASME. State University of New York at Binghamton, Department of Mechanical Engineering) pp 173–9
[30] Rahaman A and Kim B 2020 Sound source localization by *Ormia ochracea* inspired low–noise piezoelectric mems directional microphone *Sci. Rep.* **10** 1–10
[31] Miles R N, Su Q, Cui W, Shetye M, Degertekin F, Bicen B, Garcia C, Jones S and Hall N 2009 A low-noise differential microphone inspired by the ears of the parasitoid fly *Ormia ochracea J. Acoust. Soc. Am.* **125** 2013–26
[32] Susanne C, Guidotti A and Hauspie R 1985 Age changes of skull dimensions *Anthropologischer Anzeiger* **43** 31–36 (available at: www.jstor.org/stable/29539588)
[33] Groves C P 1982 The skulls of asian rhinoceroses: wild and captive *Zoo Biol.* **1** 251–61
[34] Tollin D J and Koka K 2009 Postnatal development of sound pressure transformations by the head and pinnae of the cat: monaural characteristics *J. Acoust. Soc. Am.* **125** 980–94
[35] Katsaros C, Berg R and Kiliaridis S 2002 Influence of masticatory muscle function on transverse skull dimensions in the growing rat *J. Orofac. Orthop./Fortschritte der Kieferorthopädie* **63** 5–13
[36] Schindelin J *et al* 2012 Fiji: an open-source platform for biological-image analysis *Nat. Methods* **9** 676–82
[37] Rolfe S, Pieper S, Porto A, Diamond K, Winchester J, Shan S, Kirveslahti H, Boyer D, Summers A and Maga A M 2021 Slicermorph: An open and extensible platform to retrieve, visualize and analyse 3d morphology *Methods Ecol. Evol.* **12** 1816–25
[38] Fedorov A *et al* 2012 3d slicer as an image computing platform for the quantitative imaging network *Magn. Reson. Imaging* **30** 1323–41
[39] 3D Slicer image computing platform 2022 (available at: www.slicer.org/)
[40] Liu H, Currano L, Gee D, Helms T and Yu M 2013 Understanding and mimicking the dual optimality of the fly ear *Sci. Rep.* **3** 1–6
[41] Reid A, Marin-Cudraz T, Windmill J F and Greenfield M D 2016 Evolution of directional hearing in moths via conversion of bat detection devices to asymmetric pressure gradient receivers *Proc. Natl Acad. Sci.* **113** E7740–8
[42] Doke J GRABIT 2023 (available at: www.mathworks.com/matlabcentral/fileexchange/7173-grabit/)
[43] Socha J J and De Carlo F 2008 Use of synchrotron tomography to image naturalistic anatomy in insects *Developments in X-Ray Tomography VI* vol 7078 (SPIE) pp 82–88
[44] Mikel-Stites M R and Staples A E 2021 Ormia ochracea hearing model software (v1.0.0) (https://doi.org/10.5281/zenodo.5590043)
[45] van Hemmen J L, Christensen-Dalsgaard J, Carr C E and Narins P M 2016 Animals and ice: meaning, origin and diversity *Biol. Cybern.* **110** 237–46
[46] Rosowski J J and Saunders J C 1980 Sound transmission through the avian interaural pathways *J. Comp. Physiol.* **136** 183–90
[47] Muller P and Robert D 2001 A shot in the dark: the silent quest of a free-flying phonotactic fly *J. Exp. Biol.* **204** 1039–52
[48] Zuk M, Rotenberry J T and Tinghitella R M 2006 Silent night: adaptive disappearance of a sexual signal in a parasitized population of field crickets *Biol. Lett.* **2** 521–4
[49] Pascoal S, Cezard T, Eik-Nes A, Gharbi K, Majewska J, Payne E, Ritchie M G, Zuk M and Bailey N W 2014 Rapid convergent evolution in wild crickets *Curr. Biol.* **24** 1369–74
[50] Gray D A, Banuelos C, Walker S E, Cade W H and Zuk M 2007 Behavioural specialization among populations of the acoustically orienting parasitoid fly *Ormia ochracea* utilizing different cricket species as hosts *Animal Behav.* **73** 99–104
[51] Walker T and Wineriter S 1991 Hosts of a phonotactic parasitoid and levels of parasitism (Diptera: Tachinidae: *Ormia ochracea*) *Florida Entomol.* **74** 554–9
[52] Lakes-Harlan R, Stölting H and Stumpner A 1999 Convergent evolution of insect hearing organs from a preadaptive structure *Proc. R. Soc.* B **266** 1161–7
[53] Robert D, Miles R N and Hoy R 1999 Tympanal hearing in the sarcophagid parasitoid fly *Emblemasoma sp.*: the biomechanics of directional hearing *J. Exp. Biol.* **202** 1865–76